Int. J. Nanosci. Nanotechnol., Vol. 19, No. 4, Dec. 2023, pp. 277-293
DOI: 10.22034/ijnn.2023.2000528.2367

Investigation of the Structural and Thermodynamic Parameters on the Nonlinear Optical Properties of InGaAs/InP Triple Quantum Well Exposed to an External Electric Field

Muhammed Sayrac[1], Hassen Dakhlaoui[2,3], Miguel Eduardo Mora-Ramos[4] and Fatih Ungan[5,*]

[1]Department of Nanotechnology Engineering, Sivas Cumhuriyet University, P. O. Box 58140 Sivas, Turkey
[2]Nanomaterials Technology unit, Basic and Applied Scientific Research Center (BASRC), College of Science of Dammam, Imam Abdulrahman Bin Faisal University, P. O. Box 1982, 31441 Dammam, Saudi Arabia
[3]Department of Physics, College of Sciences for Girls, Imam Abdulrahman Bin Faisal University, Saudi Arabia
[4]Centro de Investigación en Ciencias-IICBA, Universidad Autonoma del Estado de Morelos, Ave. Universidad P. O. Box 51001, CP 62209, Cuernavaca, Morelos, Mexico
[5]Department of Physics, Sivas Cumhuriyet University, P. O. Box 58140 Sivas, Turkey

(*) Corresponding author: fungan@cumhuriyet.edu.tr
(Received: 25 April 2023 and Accepted: 10 October 2023)

Abstract

In this study, the effects of both tunable physical parameters and thermodynamic variables on the linear and nonlinear optical properties of the InGaAs/InP triple quantum well are theoretically investigated in detail. In addition, the effect of an external static electric field applied parallel to the growth direction of the structure was also studied. To carry out this analysis, firstly, the energy eigenvalues and eigenfunctions of the system were obtained as a result of solving the time-independent Schrödinger equation using the diagonalization method, under the effective mass and envelope function approach. Then, using these energy eigenvalues and eigenfunctions, the nonlinear optical properties of the structure were calculated from the expressions derived within the compact density matrix approach via the iterative method. The effect of adjustable structure parameters and applied external fields affects the difference in subband energy levels at which transitions occur and the magnitudes of the dipole moment matrix elements. These changes in the electronic properties of the structure cause the peak positions of the total (linear plus nonlinear) optical absorption coefficient and total relative refractive index change coefficient (RRIC) to shift towards lower or higher energy regions. These results are expected to enable the proper design of new optoelectronic devices.

Keywords: *InGaAs/InP quantum well, Hydrostatic pressure, Temperature, External electric field.*

1. INRODUCTION

Nonlinear optics is a field of study that deals with the interaction between light and matter in materials that do not exhibit linear optical properties. Nonlinear optical materials are those that can exhibit nonlinearity in their response to light, meaning that the relationship between the intensity of light is not proportional [1-3]. The rapid development of nonlinear optics in recent decades has led to the discovery and development of a wide range of nonlinear optical materials. These materials have unique properties that make them useful for a variety of applications in fields

such as telecommunications, imaging, sensing, the construction of optical switches, frequency converters, and other optical devices that rely on nonlinear interactions between light and matter [4-7]. Overall, the development of nonlinear optics has had a profound impact on the field of photonics and has opened up new opportunities for the development of advanced optical technologies.

The diversification of low-dimensional semiconductor nanostructures such as quantum dots (QDs), quantum wires, and quantum wells (QWs) has led to a significant amount of research in the fields of condensed matter physics and optoelectronics. These semiconductor nanostructures have unique electrical and optical properties that arise due to their small size and quantum confinement effects. For example, the QDs exhibit discrete energy levels due to their small size, which can be used for a range of applications such as single photon sources, biological labeling [4-9]. Similarly, quantum wires and QWs have been studied for their ability to confine electrons in two or one dimensions, resulting in novel electrical and optical properties. These structures have been explored for applications such as high-speed electronics, high-efficiency solar cells, and light-emitting devices [4-7].

In recent years, there have been several studies that put forward configurations with different semiconductor structural parameters and different geometries to improve the optical and electronic properties of these structures [10-15]. Mahrsia et al. investigated nonlinear optical properties of InAs/GaAs QDs exposed to hydrostatic pressure and temperature [16]. Makhlouf et al. investigated the linear and nonlinear optical properties of InAs/GaAs structures [17]. Dahiya et al. explored the effects of temperature and hydrostatic pressure on the optical properties of semi-parabolic QD [18]. The optical properties of quantum structures have been controlled, also, due to electron localization. Optical and electric properties of single or double QWs were studied under hydrostatic pressure and temperature [19]. The optical properties of a step QW structure [20] and the optical properties of InAs/InP QWs within a tight-binding model [21] have been investigated. In addition to the theoretical studies, experimental investigations on the semiconductor structures have been reported [22]. Third-order nonlinear susceptibility was designed by molecular-beam epitaxy (MBE) [23], and intersubband transition was calculated [24].

The development of technological devices depends on the improvement of the physical and electric properties of low-dimensional semiconductor structures. The configurational setup of the semiconductor structure directly affects the physical properties of these nanosystems [25-29], namely the structure parameters, applied external fields, temperature, and hydrostatic pressure [30-32]. The investigations of the total optical absorption coefficient (TOAC) and total relative refractive index change coefficient (TRIC) of InGaAs/InP QW structures are relevant, for a variety of reasons, in the field of optics and photonics [33, 34]. These quantities provide valuable information about the properties of a material, including its electronic structure and composition. The investigation of TOACs and TRICs becomes an important area of research, with a wide range of practical applications regarding the behavior of light in materials. The TOACs and TRICs are crucial parameters for designing optical devices, such as solar cells, LEDs, and optical fibers. By accurately measuring these parameters, optimization of the performance of these devices and efficiency could be achieved.

Based on these studies, this paper aims to expose the role of the TOACs and TRICs in triple InGaAs/InP QW potentials. For analyzing these parameters, firstly, the energy eigenvalues and eigenfunctions of

the structure are obtained, within the framework of effective mass and parabolic band approximations, under different structure parameters and external probes such as temperature, hydrostatic pressure and static electric fields. Then, the compact density matrix approximation is applied to produce evaluating expressions for the nonlinear optical properties of the structure. The organization of the paper is as follows: Section 2 draws a theoretical framework. Section 3 discusses the numerical results. Section 4 presents the conclusion of the paper.

2. THEORY

This study investigates how the nonlinear optical properties of an InxGa1-xAs/InP triple quantum well (TQW) are affected by structural parameters and external probes.

The schematic presentation of the TQW structure is given in Figure 1. This structure consists of three thin layers of InGaAs sandwiched between two wider layers of InP. The InGaAs layers are the QWs, where electrons are confined in the vertical direction, while the InP layers act as barriers, preventing the electrons from escaping. The configuration of the structure stetting: z_1=3nm, z_2-z_1 = Lw_L, z_3-z_2 = Lb_L, z_4-z_3 = Lw_C, z_5-z_4 = Lb_R, z_6-z_5 = Lw_R, z_7-z_6= 3nm. V_0= 518meV (quantum well depth for the composition of x=0.53). Lw_L, Lw_C, Lw_R, Lb_L, and Lb_R are left well width, center well width, right well width, left barrier thickness, and right barrier thickness, respectively.

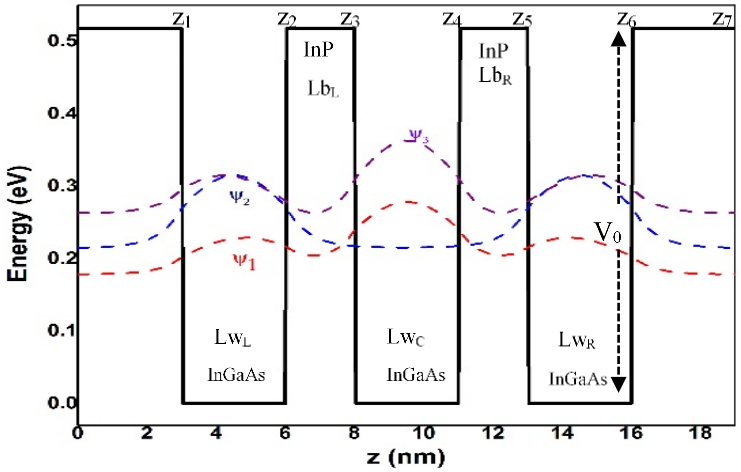

Figure 1. *The TQW structure and the corresponding wavefunctions. InGaAs /InP structure is sandwiched between the InP layer. Lw_L: left well-width, Lw_C: center well-width, Lw_R: right well-width, Lb_L: left barrier thickness, Lb_R: right barrier thickness, V_0: quantum well depth.*

The optical properties of a material are related to its electronic band structure, and the band structure of a QW is highly sensitive to external perturbations such as temperature and pressure. The thermodynamic parameters affect energy levels and wavefunctions, and so the nonlinear optical properties vary with the applied thermodynamic parameters. The total Hamiltonian of an electron confined in the proposed structure in the presence of the applied external z-oriented electric field within the framework of effective mass and parabolic band approximations are given by [35-37]

$$H = \frac{\vec{p}_e^{\,2}}{2m^*(\mathrm{P},\mathrm{T})} + V(z,P,T) - eF\vec{z} \qquad (1)$$

where $m^*(P, T)$ is the electron effective mass, P_e is the electron momentum, F is the magnitude of the applied external electric field, and the z-axis is the growth direction of the structure. The hydrostatic pressure (P) and temperature (T)

dependency of electron effective mass is given

$$m^*(\mathrm{P,T}) = \left[1 + E_P^{\Gamma}\left(\frac{2}{E_g^{\Gamma}(\mathrm{P,T})} + \frac{1}{E_g^{\Gamma}(\mathrm{P,T}) + 0.341}\right)\right]^{-1} m_0 \quad (2)$$

here m_0 is the free electron mass [38]. The mismatch of effective mass and dielectric constant is a critical factor in determining the strength and behavior of nonlinear optical effects in materials. When the intensity of light becomes sufficiently high, the response of the material to the electric field can deviate significantly from the linear behavior observed at lower intensities. This nonlinear response is rooted in the intricate interplay between the effective mass of charge carriers (often electrons) in the material and its dielectric properties. Effective mass characterizes how these charge carriers respond to external forces, like an electric field, in a crystalline lattice. The dielectric constant, on the other hand, quantifies the ability of a material to polarize in response to an electric field.

In addition, $E_g^{\Gamma}(\mathrm{P,T})$ is the energy gap (eV) for InP depending on the pressure and temperature.

$$E_g^{\Gamma}(\mathrm{P,T}) = E_g^0(0,\mathrm{T}) + \alpha P - \beta P^2(\mathrm{eV}) \quad (3)$$

where $\alpha = 8.4 \times 10^{-3}$ and $\beta = 1.8 \times 10^{-5}$ are the pressure coefficients for InP [39]. $E_g^{\Gamma}(0,\mathrm{T})$ is the temperature dependence of the energy gap, and given as

$$E_g^{\Gamma}(0,\mathrm{T}) = 1.421 + \eta T^2(\mathrm{T}+\mathrm{c})^{-1}(\mathrm{eV}) \quad (4)$$

where $\eta = 4.9 \times 10^{-4}$ and $c = 327K$ are the temperature coefficients for InP [39]. Energy band gap for InGaAs is $E_g(x,T) = 0.42 + 0.625x - [5.8/(T+300) - 4.19/(T+271)] \times 10^{-4} T^2 x - 4.19 \times 10^{-4} T^2/(T+271) + 0.475x^2(eV)$

The pressure dependence of energy band gap for InGaAs is $E_g(0.47,P) \approx (0.733 + 11\mathrm{x}10^{-3}\mathrm{P} - 27\mathrm{x}10^{-6}P^2)$ eV [40].

The pressure coefficient that for every increase in pressure of 1GPa (giga-pascal), the bandgap of InP will vary by approximately 0.07eV. Similarly, the temperature coefficient means that for every increase in 1 Kelvin (K) of temperature, the bandgap of InP changes by approximately 0.5 meV [38].

The confining potential also is affected by the temperature and the pressure and is given by

$$V(\mathrm{z,P,T}) = G_{c(v)}\left(\mathrm{E}_g^{InP}(\mathrm{P,T}) - \mathrm{E}_g^{InGaAs}(\mathrm{P,T})\right) \quad (5)$$

where the conductance and valance band offset parameters ($G_{c(v)}$) is assumed to remain constant with pressure for InP/InGaAs. The ratio is taken as 0.38:0.62 [41, 42].

With all this, the expression for $V=V(z,P,T)$, the confinement potential for the electron in the z-direction is:

$$V = \begin{cases} V_0(z,P,T) & 0 < z < z_1 \\ 0 & z_1 < z < z_2 \\ V_0(z,P,T) & z_2 < z < z_3 \\ 0 & z_3 < z < z_4 \\ V_0(z,P,T) & z_4 < z < z_5 \\ 0 & z_5 < z < z_6 \\ V_0(z,P,T) & z_6 < z < z_7 \end{cases} \quad (6)$$

In a QW structure, the bandgap energy of the material is modified by the thickness of the well, which determines the confinement of the electrons and holes within the well. If the hydrostatic pressure is applied to the structure, the lattice constant of the material changes, which can alter the bandgap energy and affect the width of the QW. The QW-width as a function of the hydrostatic pressure is given [43]

$$L(P) = L(0)\left(1 - (\mathrm{S}_{11} + 2\mathrm{S}_{12})\mathrm{P}\right) \quad (7)$$

here $L(0)$ is the QW width without hydrostatic pressure, and S_{11} and S_{22} elastic constants for InGaAs are given below [42].

$$\begin{aligned} S_{11} &= \frac{C_{11} + C_{12}}{(\mathrm{C}_{11} - \mathrm{C}_{12}) * (\mathrm{C}_{11} + 2\mathrm{C}_{12})}; \\ S_{12} &= \frac{-C_{12}}{(\mathrm{C}_{11} - \mathrm{C}_{12}) * (\mathrm{C}_{11} + 2\mathrm{C}_{12})} \\ C_{11} &= \left(8.34 + 3.56 * x\right) * 10; \\ C_{12} &= (4.54 + 0.80 * x) * 10 \end{aligned} \quad (8)$$

The subband energy levels and the corresponding wave functions of the electrons in this structure can be calculated using the time-independent Schrödinger equation. The wave function of an electron

in a QW can be described as a standing wave. The wavefunction in the barriers is an exponential decay function, with the amplitude decreasing rapidly as the electron moves away from the well. The exact form of the wavefunctions depends on the thicknesses and compositions of the layers, as well as the energy level of the electrons. These wavefunctions are important in understanding the optical and electrical properties of the structure, such as the absorption and emission of light, and the transport of electrons through the structure. The different structure parameters and the applied external fields cause the variation of the subband energy levels and the corresponding wave functions. We used the diagonalization method [44] to calculate this change in the electronic structure of the system. In this method, the calculation of the single-electron wave function $\psi(z)$ is performed for infinite quantum well width L_∞, which is large compared to the triple QW widths. The wave function describing the structure is given

$$\psi(z)=\sqrt{\frac{2}{L_\infty}}\sum_{m=1}^{\infty}C_m \sin(m\pi[\frac{z}{L_\infty}+\frac{1}{2}]) \quad (9)$$

After the hydrostatic pressure and temperature-dependent structural parameters are defined, the energies and corresponding wave functions can be obtained by solving Eq. (1) by the method described above. Then, the linear, third-order nonlinear, and total optical absorption coefficients (TOACs), and total refractive index changes (TRICs) for transition for the electron states are analytically expressed under the compact density matrix approach and iterative method [45].

The absorption coefficient and refractive index changes are defined as [45].

$$\beta(\omega)=\omega\sqrt{\frac{\mu}{\varepsilon_R}}\,\mathrm{Im}[\varepsilon_0\chi(\omega)] \quad (10)$$

$$\frac{\Delta n(\omega)}{n_r}=\mathrm{Re}[\frac{\chi(\omega)}{2n_r^2}] \quad (11)$$

Now we can give the analytical formula for the linear and third-order nonlinear absorption coefficients and relative refractive index changes. These expressions are defined as follows [46, 47]

$$\beta^{(1)}(\omega)=\omega\sqrt{\frac{\mu}{\varepsilon_r}}\frac{|M_{10}|^2\sigma_v\hbar\Gamma_{10}}{(E_{10}-\hbar\omega)^2+(\hbar\Gamma_{10})^2} \quad (12)$$

$$\frac{\Delta n^{(1)}(\omega)}{n_r}=\frac{\sigma_v|M_{10}|^2}{2n_r^2\varepsilon_0}\left[\frac{E_{10}-\hbar\omega}{(E_{10}-\hbar\omega)^2+(\hbar\Gamma_{10})^2}\right] \quad (13)$$

$$\beta^{(3)}(\omega,I)=-2\omega\sqrt{\frac{\mu}{\varepsilon_r}}\left(\frac{I}{\varepsilon_0 n_r c}\right)\frac{|M_{10}|^4\sigma_v\hbar\Gamma_{10}}{[(E_{10}-\hbar\omega)^2+(\hbar\Gamma_{10})^2]^2}\left[1-\frac{|M_{11}-M_{00}|^2}{|2M_{10}|^2}\times\frac{(E_{10}-\hbar\omega)^2-(\hbar\Gamma_{10})^2+2(E_{10})(E_{10}-\hbar\omega)}{(E_{10})^2+(\hbar\Gamma_{10})^2}\right]. \quad (14)$$

$$\frac{\Delta n^{(3)}(\omega,I)}{n_r}=-\frac{\mu c|M_{10}|^2}{4n_r^3\varepsilon_0}\frac{\sigma_v I}{[(E_{10}-\hbar\omega)^2+(\hbar\Gamma_{10})^2]^2}\times\left[4(E_{10}-\hbar\omega)|M_{10}|^2-\frac{(M_{11}-M_{00})^2}{(E_{10})^2+(\hbar\Gamma_{10})^2}\{(E_{10}-\hbar\omega)\times[(E_{10})(E_{10}-\hbar\omega)-(\hbar\Gamma_{10})^2]-(\hbar\Gamma_{10})^2(2(E_{10})-\hbar\omega)\}\right] \quad (15)$$

where ω presents the angular frequency and Γ is the relaxation time for intersubband transitions. μ and ε_r are magnetic permeability and the real part of the electrical permittivity. σ_v is the carrier density, $\hbar$ is the Planck constant and n_r is the refractive index. E_{ij} is the i^{th} and j^{th} energy state of the electron. M_{ij} corresponds to transition dipole element.

The total TOACs and TRICs equal the sum of the linear and third-order nonlinear terms and are given by the following equation:

$$\beta(\omega,I)=\beta^{(1)}(\omega)+\beta^{(3)}(\omega,I) \quad (16)$$

and

$$\frac{\Delta n(\omega,I)}{n_r} = \frac{\Delta n^{(1)}(\omega)}{n_r} + \frac{\Delta n^{(3)}(\omega,I)}{n_r} \quad (17)$$

where the relative refractive index of the system is $n_r = \sqrt{\varepsilon_r}$ and the real part of the permittivity is $\varepsilon_R = n_r^2 \varepsilon_0$. ε_0 and μ_0 are vacuum permittivity and vacuum permeability, respectively. σ_υ is the carrier density of the system. ω is the angular frequency of the incident photon, I is the optical intensity of the incident photon, E_{10} is the energy difference between the two lowest energy levels and Γ_{10} is defined as the relaxation rate for states 1 and 0. $M_{ij} = \langle \psi_i(z)|ez|\psi_j(z)\rangle$ (here i,j=0,1) represents the dipole moment matrix element for the transitions.

3. RESULT AND DISCUSSION

The applied external probes (hydrostatic pressure, temperature, and external electric field) on the nonlinear optical properties of the triple InGaAs/InP structure have been investigated. The effective mass and compact density matrix approaches are used for the calculation of nonlinear optical properties. The simulation parameters are [48]: $m^* = 0.077m_0$ where m_0 is the mass of a free electron, e= $1.602x10^{-19}C$, c=$3x10^8 m/s$, ħ= $1.056x10^{-34}Js$, ε_0=$8.854x10^{-12}C^2/Nm^2$, μ=$4\pi\times10^{-7}$ Hm^{-1}, σ_V=$3.0x10^{22}m^{-3}$, x=0.53, V_0=$518meV$, n_r~(3.27) is the refractive index of $In_xGa_{1-x}As$/InP at a composition of 0.53. The use of a uniform effective mass in the whole structure of InP/InGaAs is based on the assumption that the energy bands and electronic properties of the material are uniform throughout the structure. This is a reasonable approximation in many cases, as long as the composition and doping levels of the material are kept relatively constant. The effective mass approximation assumes that the electron and hole masses are uniform throughout the material, which allows for simpler calculations of electronic properties and band structure.

In the first stage of the study, the electronic and optical properties of the $In_xGa_{1-x}As$/InP TQW structure were investigated for different barrier thicknesses. The composition of the $In_xGa_{1-x}As$ alloy is parameterized by x, which ranges from 0 to 1 and determines the bandgap energy of the material. For the specific TQW structure with x=0.53, the bandgap energy (V_0) is 518 meV. With this composition, the alloy is lattice matched to InP. Besides, the thickness of the barriers in the TQW structure plays an important role in determining the electronic and optical properties of the material. As the barrier thickness increases, the interactions of electrons trapped inside the QWs decrease, which affects the quantum mechanical properties of the system. With the increase of the barrier thickness too much, the structure behaves like three single -isolated- QWs that do not interact with each other. As a result, the energy levels of the electrons in the QWs become more closely spaced, and the overlap between the wavefunctions of adjacent QWs increases. The numerical results of the dipole moment matrix elements and the energy difference between the subband energy levels are given in Table 1.

Table 1. *Energy difference and dipole moment matrix element for InGaAs/InP structure at the different left barrier and right barrier thickness (Lb_L=Lb_R =2, 3, 4, 5nm). Left, center, and right QW-width are set to 3nm (Lw_L=Lw_C=Lw_R = 3nm). The external fields are set to zero (T = 300K, P = F = 0).*

Lb_L=Lb_R (nm)	E_{10} (meV)	M_{10}(nm)	$\lvert M_{10}\rvert^2 x E_{10}$ (nm^2xmeV)
2	36.8140	3.5392	461.13
3	17.8196	4.1789	311.187
4	8.7521	4.7669	198.877
5	4.4475	5.2041	120.4501

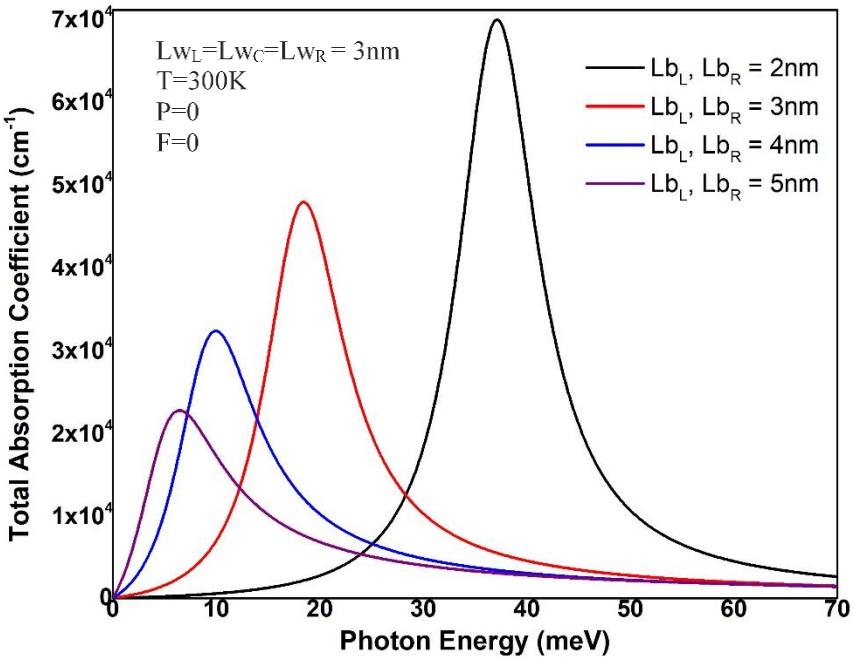

Figure 2. *The change of total optical absorption coefficients for different barrier thicknesses.*

Figure 2 shows the variation of the total optical absorption coefficient of the TQW structure versus the incident photon energy for different barrier thicknesses. The quantum well widths considered are equal to 3nm. The applied external fields (hydrostatic pressure, and electric field) are set to zero, and the temperature is kept at 300K. The increment of left and right barrier thickness results in the red shift of the resonant peak of TOAC because the ground and first excited state energy values are diminished with the increment of barrier thickness, (see Table 1). The total optical absorption coefficient is a measure of the absorption of light by a material. The absorption coefficient is proportional to the transition probability per unit of time between two states of the material. The energy difference between the ground state and the first excited state is an important factor that affects the absorption coefficient. The amplitude of the total optical absorption coefficient is proportional to the product of the square of the dipole moment matrix element with the energy difference ($|M_{10}|^2 x E_{10}$). In Table 1, $|M_{10}|^2 x E_{10}$ decreases with the increment of the barrier thickness so the amplitude of TOAC decreases with the increment of barrier thickness. Furthermore, we observe in Fig. 2 that the amplitude of the TOAC diminishes considerably by augmenting the barrier widths Lb_L and Lb_R from 2 to 3 nm. However, it decreases for Lb_L and Lb_R from 4 to 5 nm. This result is because when the left and right barrier widths take higher values, the quantum wells become decoupled and not sensitive to the effects of barrier widths, per a consequence, the wavefunctions spread will be less sensitive to further increase of barrier widths which explains the small reduction of the (TOAC) amplitude when Lb_L and Lb_R from 4 to 5nm.

Figure 3 exhibits total refractive index change (TRIC) at different barrier thicknesses (L_b). The quantum barrier widths, temperature, hydrostatic pressure, and external electric field are kept constant. This quantity is largely dependent on the energy level structure in the QW as well as on the corresponding electron wave functions, which are closely related to the geometry of confining potential. In this sense, both the energy position of its nodes and the amplitude of the extrema are affected by changes in well and barrier region widths. The barrier thickness variation causes a decrease in the

energy levels of the confined states, and this results in the red shift of the resonant peak of the TRIC. The magnitude of the refractive index change caused by the interaction between light and matter is related to the strength of the interaction. The strength of the interaction is related to the dipole moment matrix element (M_{10}). M_{10} is a fundamental quantity that determines the strength of the interaction between light and matter, and therefore, it determines the magnitude of the refractive index change. M_{10} increases with the increment of barrier thickness, Table 1. This increment causes a rise in the amplitude of TRIC. Furthermore, we observe that for all values of Lb_L and Lb_R, the (TRICs) display a similar behavior. They increase at first, reach their maximum, and then diminish rapidly, intercept the zero axis, and reach again their minimum. After that, all (TRICs) tend progressively to zero energy.

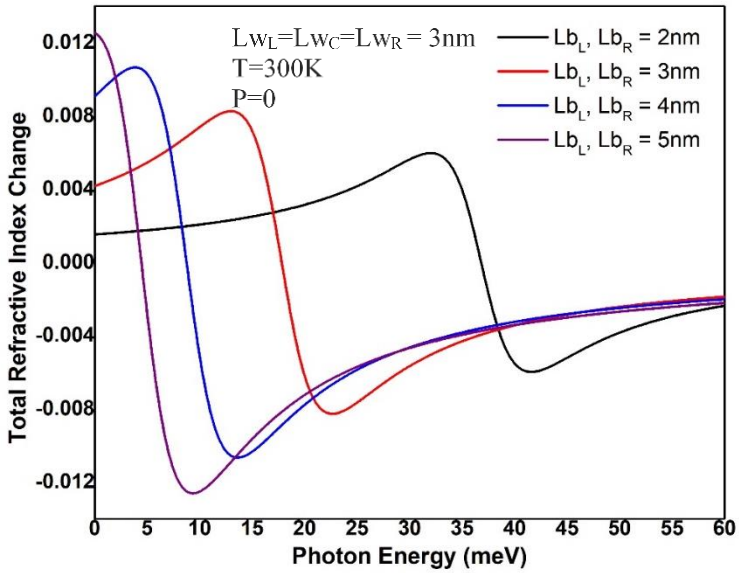

Figure 3. *Total refractive index change at different left and right barrier thicknesses.*

Table 2. *Energy levels of confined states and the diple moment matrix elements for InGaAs/InP structure at different quantum well widths.*

$Lw_L=Lw_C=Lw_R$ (nm)	E_{10} (meV)	M_{10}(nm)	$\|M_{10}\|^2xE_{10}$ (nm^{2}xmeV)
4	11.1970	4.8722	265.798
5	7.5179	5.5668	232.974
6	5.3070	6.2618	208.088
7	3.7942	6.8570	178.397

Table 2 gives the energy levels of confined states and the diple moment matrix elements for the TQW structure at the different left, center, and right barrier well thicknesses ($Lw_L=Lw_C=Lw_R$), i.e. the symmetry of the TQW structure does not change. Left and right barrier thicknesses (L_b) are kept constant at 3nm. The temperature, hydrostatic pressure, and electric field are kept constant (T=300K, P=F=0). Figure 4 demonstrates the total absorption coefficient of InGaAs/InP triple quantum well structure for different quantum well widths. The quantum barrier thicknesses are taken to be equal to 3nm. The applied external probes (hydrostatic pressure, and electric field) are set to zero, and the temperature is 300K. As the width of the quantum wells increases, the wave functions of the electrons become more spread out and so the energy levels of the structure are lowered due to the reduced confinement of the electrons. At the same time, the inter-level transition energy goes

down. This results in a redshift of the resonant absorption peak position of the TQW structure. The amplitude of TOAC is proportional to the product of transition probability (square of dipole moment matrix element or ($|M_{10}|^2$) and the energy difference (E_{10}). The product of transition probability with the energy difference ($|M_{10}|^2 x E_{10}$) decreases with the increment of the barrier widths, as noticed in Table 2. Thus, the resonant peak amplitude of the TOAC decreases with the increment of QW widths.

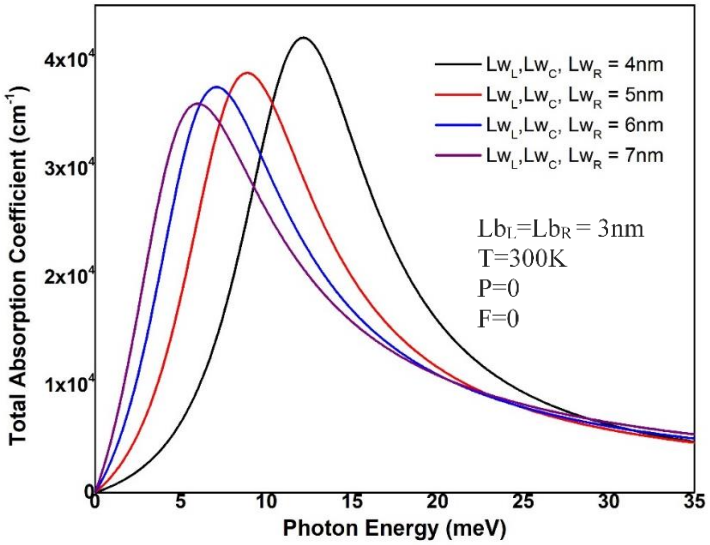

Figure 4. *Change in total optical absorption coefficients at different quantum well widths.*

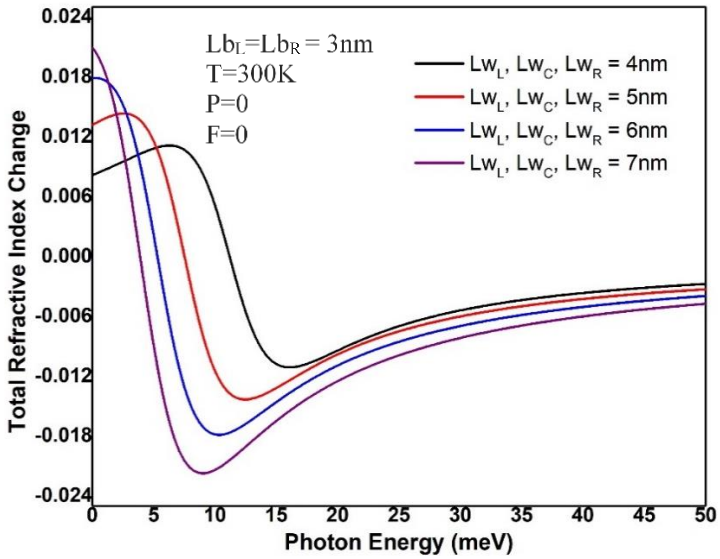

Figure 5. *Total refractive index change at different quantum well widths.*

In Figure 5, the maximum peak position of the TRIC in a InGaAs/InP TQW shifts to a lower energy region due to an increase in the quantum well widths. The quantum barrier thickness is set to 3nm as well. The applied external probes (hydrostatic pressure, and electric field) are set to zero. The temperature is kept at 300K. The resonant peak position of the TRIC corresponds to the energy at which the electrons in the structure undergo a transition between energy states. An increase in the quantum well width leads to a redshift in the resonant peak position of the TRIC because a wider well leads to a diminished transition energy, as presented

in Table 2. As discussed, the amplitude of TRIC depends on the dipole moment matrix element (M_{10}). M_{10} increases with the increment of quantum well widths, Table 2. For this reason, the magnitude of TRIC coefficients increases with the increment of QW widths.

Table 3. *Energy levels and dipole moment matrix elements at different temperatures.*

T (K)	E_{10}(meV)	M_{10}(nm)	$\|M_{10}\|^2 x E_{10}$ (nm^{2}xmeV)
100	7.3081	5.5683	226.595
300	7.5179	5.5668	232.974
500	7.8504	5.5623	242.885
700	8.3164	5.5558	256.702
900	8.8811	5.5478	273.343

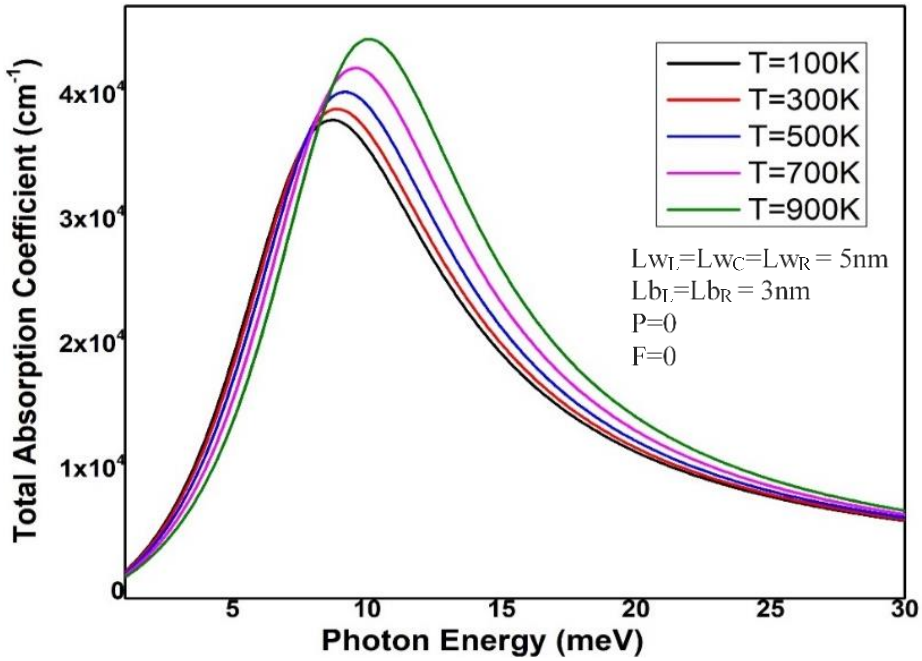

Figure 6. *Change in total optical absorption coefficients at different temperatures.*

Table 3 presents the energy values of confined states and dipole moment matrix elements at different temperatures (T=100, 300, 500, 700, 900 K). Quantum well widths are set to 5nm and barrier thicknesses are set to 3nm. The external hydrostatic pressure and electric field are taken to be zero.

Figure 6 shows the change in total optical absorption coefficients at different temperatures. The quantum well widths (Lw_L=Lw_C=Lw_R = 5nm), quantum barriers thickness (Lb_R = Lb_L=3nm), hydrostatic pressure (P=0), and the external electric field (F=0) are kept constant. The absorption coefficient shifts to a higher energy region (blue shift) with the increment of temperature due to increased transition energy values. The amplitude of the total absorption coefficient increases with the temperature due to thermal broadening. This amplitude depends on the product of $|M_{10}|^2 x E_{10}$. This product increases with the increment of the temperature. Thus, the magnitude of the total absorption coefficient increase with the rise in temperature due to thermal effects. Furthermore, we remark that the TOAC is less sensitive to the temperature variation for small and higher values of the photon energy (E<5 meV and E>25 meV). The region for which we can distinguish the small variation of TOAC is around its peak as shown in Fig 6.

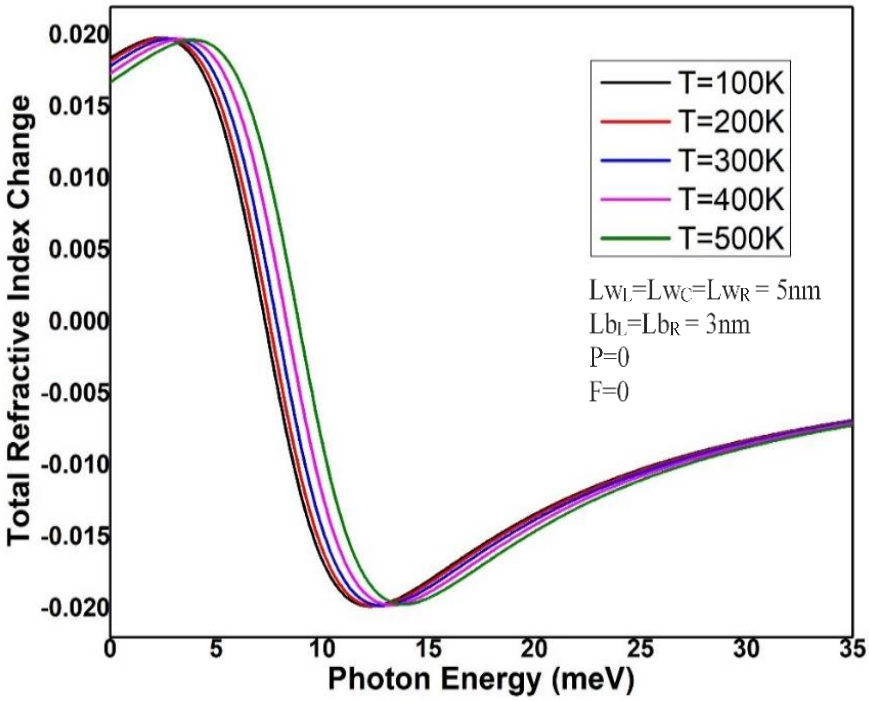

Figure 7. *Variation of total refractive index change at different temperatures.*

Figure 7 gives information about the behavior of TRIC at different temperatures for triple InGaAs/InP QW structure. The structural parameters are kept constant, namely, Lw_L=Lw_C=Lw_R =5nm, Lb_R= Lb_L=3nm, P=0, and F=0. The resonant peak position of the total refractive index change in a triple InGaAs/InP quantum well structure can shift towards blue wavelengths with increasing temperature. As the temperature increases, the bandgap energy value of the materials diminishes -although at different paces-, but there is also an effect of thermal expansion that makes the effective QW width increase. As a result, QW transition energies increment as noticed in Table 3. These changes can cause the resonant peak position to shift towards to higher energy (blueshift) region. The magnitude of total refractive index change depends on the dipole moment matrix element (M_{10}). The variation of the dipole moment matrix element is low, Table 3. Thus the magnitude variation of TRIC is not noticeable with the increment in temperature.

Table 4 gives energy values of confined states and dipole moment matrix elements as a function of applied hydrostatic pressure. QW widths, barrier thicknesses, and external fields are kept constant (Lw_L=Lw_C=Lw_R=5nm, Lb_L=Lb_R =3nm, T=300K, and F=0).

Table 4. *Variation of energy values and dipole moment matrix elements at different hydrostatic pressures.*

P (kbar)	E_{10}(meV)	M_{10}(nm)	$\|M_{10}\|^2 x E_{10}$ (nm^{2}xmeV)
0	7.5179	5.5668	232.974
10	7.0462	5.5681	218.459
20	6.6864	5.5693	207.393
30	6.2378	5.5706	193.569

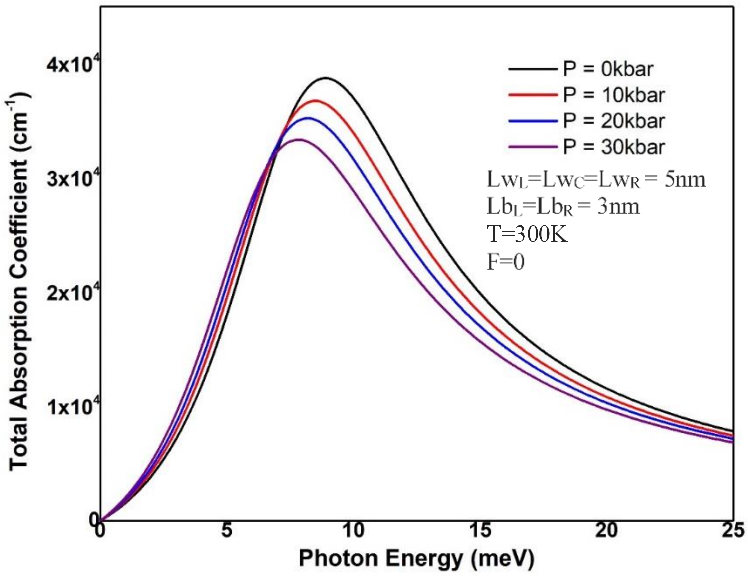

Figure 8. *Change in total optical absorption coefficients at different pressures.*

Figure 8 exhibits a change in the resonant peak position of the total optical absorption coefficient at different hydrostatic pressures. The QW width, barrier thickness, temperature, and external electric field are constant, namely, Lw_L=Lw_C=Lw_R = 5nm, Lb_R = Lb_L=3nm, T=300K, and F=0. The resonant peak in the absorption coefficient corresponds to the energy difference between the highest occupied energy level (valence band) and the lowest unoccupied energy level (conduction band). Specifically, the pressure can affect the band gap. The direct Γ-Γ band gap of the involved materials increases with the increment in hydrostatic pressure, with a much higher rate in the InAs case. This, together with the pressure-induced reduction of lattice constants, leads to the behavior of transition energies appearing in Table 4. Thus, the resonant peak in the absorption coefficient shifts to a lower energy region, resulting in a redshift. The amplitude of TOAC depends on the product of |M10|2xE10. This product decreases with the increment of hydrostatic pressure (Table 4), leading to a decrease in the amplitude of the TOAC resonant peak.

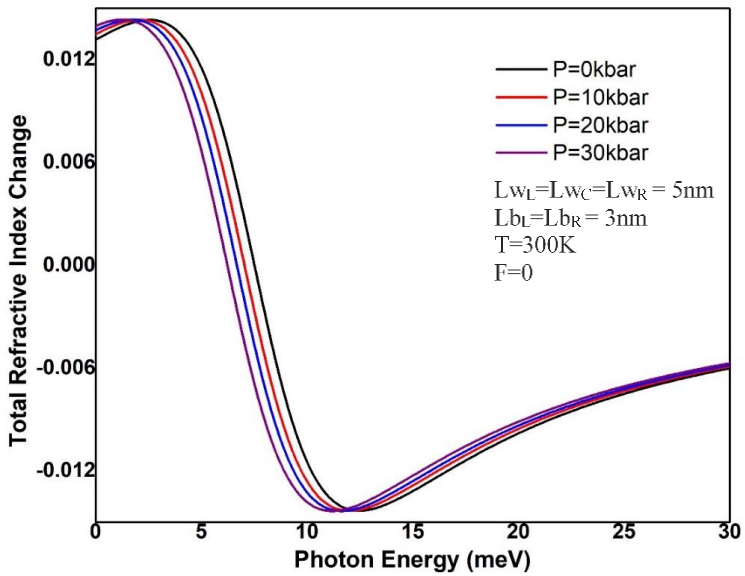

Figure 9. *Change in total refractive index change at different pressures.*

Figure 9 presents the variation of TRIC as a function of incoming photon energy for different values of hydrostatic pressure for triple InGaAs/InP QW structure. The structural parameters are kept constant, namely Lw_L=Lw_C=Lw_R = 5nm, Lb_R = Lb_L=3nm, T=0, and F=0. As commented, transition energy decreases with the increment of the hydrostatic pressure (Table 4) so the resonant peak position of TRIC redshifts to lower energies. The magnitude of TRIC depends on the dipole moment matrix element (M_{10}). This term does not change much with the hydrostatic pressure (Table 4), leading to not much noticeable change in the amplitude of TRIC.

Table 5 shows the energy values and dipole moment matrix elements with the applied external electric field (F=0, 30, 60, 90 kV/cm). The QW widths, barrier thicknesses temperature, and hydrostatic pressure are kept constant, (Lw_L=Lw_C=Lw_R=5nm, Lb_L=Lb_R=3nm, T=300K, and P=0)

Table 5. *Confined energy values and dipole moment matrix elements at different applied electric fields.*

F(kV/cm)	E_{10}(meV)	M_{10}(nm)	$\|M_{10}\|^2 x E_{10}$ (nm^{2}xmeV)
0	7.5179	5.5668	232.974
30	24.9365	2.9288	213.902
60	48.2895	1.892	172.861
90	72.0245	1.3540	132.043

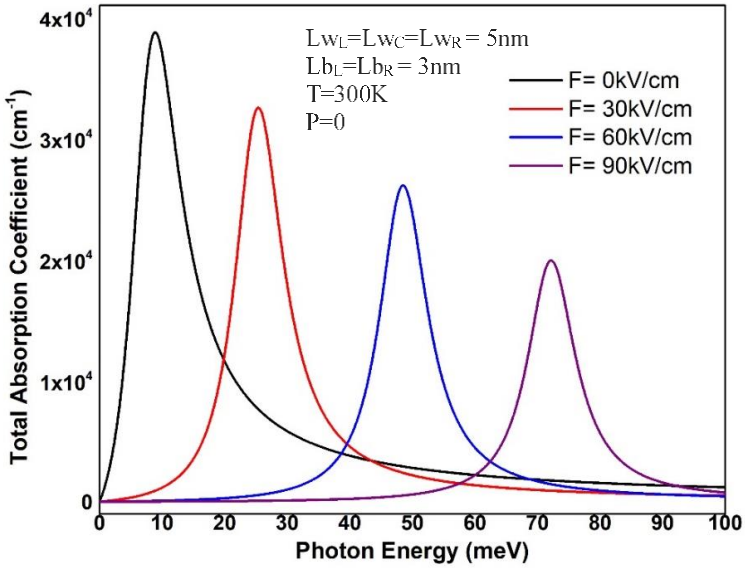

Figure 10. *Variation of total optical absorption coefficients at different applied external electric fields.*

Figure 10 details the total optical absorption coefficient in the investigated InGaAs/InP structure, for different intensities of an applied electric field. The structural parameters are kept constant, namely Lw_L=Lw_C=Lw_R = 5nm, Lb_R = Lb_L=3nm, T=300K, and P=0. The optical absorption coefficients can be tuned by applying an external electric field. Under such circumstances, it manifests the so-called quantum-confined Stark effect (QCSE). The inter-level energy difference significantly increases with the applied external electric field, (Table 5). Therefore, a blue shift of TOAC can be observed. The amplitude of TOAC is proportional to the

product of the dipole moment matrix element and energy level ($|M_{10}|^2 x E_{10}$). This product decreases with the increment of the applied electric field, Table 5, leading to a decrement in the amplitude of the TOAC resonant peak

Finally, Fig. 11 presents the TRIC for different applied external electric field values. The quantum well widths, barrier thickness, temperature, and hydrostatic pressure are kept constant, Lw_L=Lw_C=Lw_R = 5nm, Lb_R = Lb_L=3nm, T=300K, and P=0, respectively. The position of TRIC node moves to higher energy regions due to the increment of E_{10} (see Table 5). TRIC resonant peak position is blueshifted due to the increment of the confined state energy levels. The amplitude of TRIC is proportional to the dipole moment matrix element, M_{10}. This element decreases with the increment of the applied electric field, Table 5, leading to a decrease in the amplitude of the TRIC resonant peak.

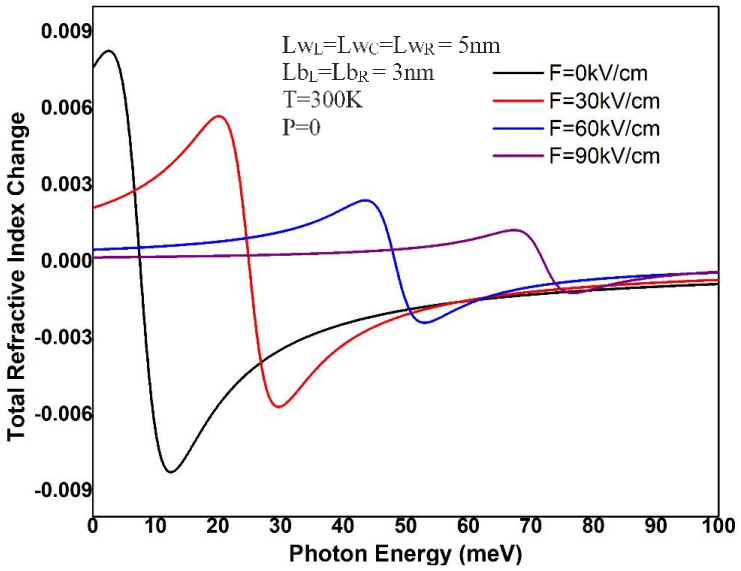

Figure 11. *Change in total refractive index change at different applied electric fields.*

4. CONCLUSION

InGaAs/InP QW structures are commonly used in optoelectronic devices such as photodetectors and modulators. In consequence, modification of the optical response of InGaAs/InP heterostructures by altering the dimensions of the quantum well structure or by the application of external probes becomes relevant. By changing the thickness or composition of the quantum well layers, the resonant peak position of nonlinear optical responses can be tuned to different wavelengths. So, the coefficients of optical absorption and relative refractive index change (TOAC and TRIC, respectively) can be increased or decreased to achieve desired levels of electro-optic activity. Also, the resonant peak position of these coefficients can be modified by changing the temperature and hydrostatic pressure of the material.

Temperature changes can affect the bandgap energy of the InGaAs/InP quantum well structure, which in turn can modify the resonant peak position. Hydrostatic pressure affects the bandgap energy and thus the resonant peak position of the InGaAs/InP quantum well structure. These modifications can be used to tune the material's optical and electro-optic properties for specific applications in photonics and optoelectronics. In addition, modification of the resonant peak position of TOAC and TRIC InGaAs/InP quantum wells by altering the applied external electric field is investigated. In addition, the resonant peak positions of the coefficients are modified by altering the applied external electric field. This is due

to the quantum-confined Stark effect (QCSE). The QCSE is a result of the spatial confinement of charge carriers in the quantum wells, leading to a modification of the electron energy levels and thus the absorption spectrum of the material.

In summary, the TOAC and TRIC of triple InGaAs/InP quantum wells can be modified by altering the thickness and composition of the quantum well layers as well as the applied external effects (temperature, hydrostatic pressure, and electric field). This can be used to tune the material's optical response and electro-optic activity for specific applications in photonics and optoelectronics.

CONFLICT OF INTEREST

The authors declare that they have no known competing financial interests or personal relationships that could have appeared to influence the work reported in this paper.

DATA AVAILABILITY STATEMENT

This manuscript has associated data in a data repository. Data will be made available on request.

REFERENCES

1. Pokutnyi, S. I., "Polarizability of germanium quantum dots with spatially separated electrons and holes in Ge/Si heterostructures", *Philosophical Magazine Letters*, 99 (2019) 386-395.
2. Bouzaïene, L., Ben Mahrsia, R., Baira, M., Sfaxi, L., Maaref, H., "Hydrostatic pressure and temperature effects on nonlinear optical rectification in a lens shape InAs/GaAs quantum dot", *Journal of Luminescence*, 135 (2013) 271-275.
3. Chen, Y. Y., Feng, X. L., Liu, C., "Generation of Nonlinear Vortex Precursors", *Physical Review Letters*, 117 (2016) 023901.
4. Ungan, F., Bahar, M. K., Barseghyan, M. G., Pérez, L. M., Laroze, D., "Effect of intense laser and electric fields on nonlinear optical properties of cylindrical quantum dot with Morse potential", *Optik*, 236 (2021) 166621.
5. Yu, Y. B., "Second-Order Nonlinear Optical Effect in an Asymmetric Quantum Well", *Applied Mechanics and Materials*, 389 (2013) 1075-1079.
6. Kaynar, E., Alaydin, B. O., "Optical properties of AlxInyGa1−x−yAs/AlzGawIn1−z−wAs quantum wells under electric and magnetic fields for telecommunication applications", *The European Physical Journal Plus*, 138 (2023) 121.
7. Feddi, E., Zouitine, A., Oukerroum, A., Dujardin, F., Assaid, E., Zazoui, M. "Size dependence of the polarizability and Haynes rule for an exciton bound to an ionized donor in a single spherical quantum dot", *Journal of Applied Physics*, 117 (2015) 064309 .
8. Kria, M., El-Yadri, M., Aghoutane, N., Pérez, L. M., Laroze, D., Feddi, E., "Forecasting and analysis of nonlinear optical responses by tuning the thickness of a doped hollow cylindrical quantum dot", *Chinese Journal of Physics*, 66 (2020) 444-452.
9. You, J. F., Zhao, Q., Zhang, Z. H., Yuan, J. H., Guo, K. X., Feddi, E., "The effect of temperature, hydrostatic pressure and magnetic field on the nonlinear optical properties of AlGaAs/GaAs semi-parabolic quantum well", *International Journal of Modern Physics B*, 33 (2019) 1950325.
10. Bouarissa, N., "Piezoelectric and electromechanical coupling constants for GaxIn1-xSb semiconducting alloys", *Philosophical Magazine Letters*, 99 (2019) 138-145.
11. Li, B., Guo, K. X., Liu, Z. L., Zheng, Y. B., "Nonlinear optical rectification in parabolic quantum dots in the presence of electric and magnetic fields", *Physics Letters A*, 372 (2008) 1337-1340.
12. Alaydin, B. O., "Effect of high bandgap AlAs quantum barrier on electronic and optical properties of In0.70Ga0.30As/Al0.60In0.40As superlattice under applied electric field for laser and detector applications", *International Journal of Modern Physics B*, 35 (2021) 2150027.
13. Altun, D., Ozturk, O., Alaydin, B.O., Ozturk, E., "Linear and nonlinear optical properties of a superlattice with periodically increased well width under electric and magnetic fields", *Micro and Nanostructures*, 166 (2022) 207225.
14. El Khamkhami, J., Feddi, E., Assaid, E., Dujardin, F., Stébé, B., Diouri, J., "Binding energy of excitons in inhomogeneous quantum dots under uniform electric field", *Physica E: Low-dimensional Systems and Nanostructures*, 15 (2002) 99-106.
15. Feddi, E., Assaid, E., Dujardin, F., Stébé, B., Diouri, J., "Magnetic Field Influence on the Polarisability of Donors in Quantum Crystallites", *Physica Scripta*, 62 (2000) 88.

16. Ben Mahrsia, R., Choubani, M., Bouzaiene, L., Maaref, H., "Nonlinear optical rectification in a vertically coupled lens-shaped InAs/GaAs quantum dots with wetting layers under hydrostatic pressure and temperature", *Journal of Alloys and Compounds*, 671 (2016) 200-207.
17. Makhlouf, D., Choubani, M., Saidi, F., Maaref, H., "Applied electric and magnetic fields effects on the nonlinear optical rectification and the carrier's transition lifetime in InAs/GaAs core/shell quantum dot", *Materials Chemistry and Physics*, 267 (2021) 124660.
18. Dahiya, S., Lahon, S., Sharma, R., "Effects of temperature and hydrostatic pressure on the optical rectification associated with the excitonic system in a semi-parabolic quantum dot", *Physica E: Low-dimensional Systems and Nanostructures*, 118 (2020) 113918.
19. Odhiambo Oyoko, H., Porras-Montenegro, N., López, S. Y., Duque, C.A., "Comparative study of the hydrostatic pressure and temperature effects on the impurity-related optical properties in single and double GaAs–Ga1–x Alx As quantum wells", *Physica Status Solidi C*, 4 (2007) 298-300.
20. Yuh, P. F., Wang, K. L., "Optical transitions in a step quantum well", *Journal of Applied Physics*, 65 (1989) 4377-4381.
21. Albe, V., Lewis, L. J., "Optical properties of InAs/InP ultrathin quantum wells", *Physica B: Condensed Matter*, 301 (2001) 233-238.
22. West, L.C., Eglash, S.J., "First observation of an extremely large-dipole infrared transition within the conduction band of a GaAs quantum well", *Applied Physics Letters*, 46 (1985) 1156-1158.
23. Sirtori, C., Capasso, F., Sivco, D. L., Cho, A. Y., "Giant, triply resonant, third-order nonlinear susceptibility X(3)3w in coupled quantum wells", *Physical Review Letters*, 68 (1992) 1010-1013.
24. Sirtori, C., Capasso, F., Faist, J., Scandolo, S., "Nonparabolicity and a sum rule associated with bound-to-bound and bound-to-continuum intersubband transitions in quantum wells", *Physical Review B*, 50 (1994) 8663-8674.
25. Kirak, M., Altinok, Y., Yilmaz, S., "The effects of the hydrostatic pressure and temperature on binding energy and optical properties of a donor impurity in a spherical quantum dot under external electric field", *Journal of Luminescence*, 136 (2013) 415-421.
26. Ozturk, E., Sokmen, I., "Nonlinear intersubband absorption and refractive index changes in square and graded quantum well modulated by temperature and Hydrostatic pressure", *Journal of Luminescence*, 134 (2013) 42-48.
27. Karabulut, I., Mora-Ramos, M. E., Duque, C. A., "Nonlinear optical rectification and optical absorption in GaAs–Ga1–xAlxAs asymmetric double quantum wells: Combined effects of applied electric and magnetic fields and hydrostatic pressure", *Journal of Luminescence*, 131 (2011) 1502-1509.
28. Mora-Ramos, M. E., Duque, C.A., Kasapoglu, E., Sari, H., Sökmen, I., "Linear and nonlinear optical properties in a semiconductor quantum well under intense laser radiation: Effects of applied electromagnetic fields", *Journal of Luminescence*, 132 (2012) 901-913.
29. Ganguly, J., Saha, S., Pal, S., Ghosh, M., "Noise-driven optical absorption coefficients of impurity doped quantum dots", *Physica E: Low-dimensional Systems and Nanostructures*, 75 (2016) 246-256.
30. Zhang, L., Xie, H. J., "Electric field effect on the second-order nonlinear optical properties of parabolic and semiparabolic quantum wells", *Physical Review B*, 68 (2003) 235315.
31. Keshavarz, A., Karimi, M. J., "Linear and nonlinear intersubband optical absorption in symmetric double semi-parabolic quantum wells", *Physics Letters A*, 374 (2010) 2675-2680.
32. Yakar, Y., Çakır, B., Özmen, A., "Calculation of linear and nonlinear optical absorption coefficients of a spherical quantum dot with parabolic potential", *Optics Communications*, 283 (2010) 1795-1800.
33. Saha, S., Pal, S., Ganguly, J., Ghosh, M., "Exploring optical refractive index change of impurity doped quantum dots driven by white noise", *Superlattices and Microstructures*, 88 (2015) 620-633.
34. Mandal, A., Sarkar, S., Ghosh, A.P., Ghosh, M., "Analyzing total optical absorption coefficient of impurity doped quantum dots in presence of noise with special emphasis on electric field, magnetic field and confinement potential", *Chemical Physics*, 463 (2015) 149-158.
35. Sakiroglu, S., Yesilgul, U., Ungan, F., Duque, C. A., Kasapoglu, E., Sari, H., Sokmen, I., "Electronic band structure of GaAs/AlxGa1−xAs superlattice in an intense laser field", *Journal of Luminescence*, 132 (2012) 1584-1588.
36. Ungan, F., Yesilgul, U., Şakiroğlu, S., Kasapoglu, E., Sari, H., Sökmen, I., "Effects of an intense, high-frequency laser field on the intersubband transitions and impurity binding energy in semiconductor quantum wells", *Physics Letters A*, 374 (2010) 2980-2984.
37. Eseanu, N., "Simultaneous effects of laser field and hydrostatic pressure on the intersubband transitions in square and parabolic quantum wells", *Physics Letters A*, 374 (2010) 1278-1285.
38. Paul, S., Roy, J. B., Basu, P. K., "Empirical expressions for the alloy composition and temperature dependence of the band gap and intrinsic carrier density in GaxIn1−xAs", *Journal of Applied Physics*, 69 (1991) 827-829.

39. Ioffe, (March/27/2023) "*InP, InP Band Structure and Carrier Concentration*", https://www.ioffe.ru/SVA/NSM/Semicond/InP/bandstr.html.
40. Ioffe, (April/14/2023) "*InGaAs, InGaAs Band Structure and Carrier Concentration*", http://www.ioffe.ru/SVA/NSM/Semicond/GaInAs/index.html.
41. Soucail, B., Voisin, P., Voos, M., Rondi, D., Nagle, J., Cremoux, B. D., "Optical investigations of the band offsets in an InGaAs-InGaAsP-InP double-step heterostructure", *Semiconductor Science and Technology,* 5 (1990) 918.
42. Başer, P., Elagoz, S., "The hydrostatic pressure and temperature effects on hydrogenic impurity binding energies in lattice matched InP/In0.53Ga0.47As/InP square quantum well", *Superlattices and Microstructures,* 102 (2017) 173-179.
43. Adachi, S., "*Properties of Group eIV, III-V and II-VI Semiconductors*", *Willey Press,* (2005).
44. Mora-Ramos, M. E., Duque, C. A., Kasapoglu, E., Sari, H., Sökmen, I., "Electron-related nonlinearities in GaAs–Ga1−xAlxAs double quantum wells under the effects of intense laser field and applied electric field", *Journal of Luminescence,* 135 (2013) 301-311.
45. Khordad, R., "Effect of position-dependent effective mass on linear and nonlinear optical properties of a cubic quantum dot", *Physica B: Condensed Matter,* 406 (2011) 3911-3916.
46. Ungan, F., Kasapoglu, E., Duque, C. A., Sari, H., Sokmen, I., "The effect of the intense laser field on the intersubband transitions in Ga1−xInxNyAs1−y/GaAs single quantum well", *Physica E: Low-dimensional Systems and Nanostructures,* 44 (2011) 515-520.
47. Ungan, F., Yesilgul, U., Kasapoglu, E., Sari, H., Sökmen, I., "Effects of applied electromagnetic fields on the linear and nonlinear optical properties in an inverse parabolic quantum well", *Journal of Luminescence,* 132 (2012) 1627-1631.
48. Ungan, F., Mora-Ramos, M. E., Duque, C. A., Kasapoglu, E., Sari, H., Sökmen, I., "Linear and nonlinear optical properties in a double inverse parabolic quantum well under applied electric and magnetic fields", *Superlattices and Microstructures,* 66 (2014) 129-135.